Assessment of the accuracy of MRI wall shear stress estimation using numerical simulations

Sven Petersson, Petter Dyverfeldt and Tino Ebbers

Linköping University Post Print

N.B.: When citing this work, cite the original article.

Assessment of the Accuracy of MRI Wall Shear Stress Estimation using Numerical Simulations

Sven Petersson MS [1,2], Petter Dyverfeldt PhD [2-4], Tino Ebbers PhD [1-3].

[1] Division of Cardiovascular Medicine, Department of Medical and Health Sciences, Linköping University, Linköping, Sweden.

[2] Center for Medical Image Science and Visualization (CMIV), Linköping University, Linköping, Sweden.

[3] Division of Applied Thermodynamics and Fluid Mechanics, Department of Management and Engineering, Linköping University, Linköping, Sweden.

[4] Department of Radiology, University of California San Francisco, San Francisco, California, USA.

Word Count: 5124

Correspondence: Sven Petersson, Division of Cardiovascular Medicine, Department of

Medical and Health Sciences, Linköping University,

SE-58185 Linköping, Sweden.

E-mail: sven.petersson@liu.se

Running title: Accuracy of MRI WSS estimation

ABSTRACT

Purpose: To investigate the accuracy of wall shear stress (WSS) estimation using MRI. Specifically, to investigate the impact of different parameters and if MRI WSS estimates are monotonically related to actual WSS.

Materials and Methods: The accuracy of WSS estimation using methods based on phase-contrast (PC) MRI velocity mapping, Fourier velocity encoding (FVE) and intravoxel velocity standard deviation mapping were studied using numerical simulations. The influence of spatial resolution, velocity encoding, wall segmentation and voxel location were investigated over a range of WSS values.

Results: WSS estimates were found to be sensitive to parameter settings in general and spatial resolution in particular. All methods underestimated WSS, except for the FVE-based method, which instead was extremely sensitive to voxel position relative to the wall. Methods utilizing PC-based WSS estimation with wall segmentation showed to be accurate for low WSS, but were sensitive to segmentation errors.

Conclusion: Even in the absence of noise and for relatively simple velocity profiles, MRI WSS estimates can not always be assumed to be linearly or even monotonically related to actual WSS. High WSS values cannot be resolved and the estimates depend on parameter setting. Nevertheless, distinguishing areas of low and moderate WSS may be feasible.

Key words: wall shear stress, phase contrast magnetic resonance imaging, atherosclerosis, hemodynamics, Fourier velocity encoding, numerical simulations.

INTRODUCTION

Ample evidence supports the hypothesis that wall shear stress (WSS), the frictional force of the flowing blood on the vessel wall, is involved in the pathogenesis of atherosclerosis and aneurysms (1-6). Consequently, there is a great interest in the non-invasive measurement of WSS in the human arterial tree.

For Newtonian fluid flow WSS is defined as

$$WSS = \mu \left(\frac{\partial v}{\partial x} \right)_{x=0} \qquad \text{[Eq. 1]}$$

where μ is the dynamic viscosity, v is the velocity parallel to the wall and x is the distance from the wall in the direction of the wall's inward normal.

Phase-contrast (PC) magnetic resonance imaging (MRI) velocity mapping has the capability of providing spatially and temporally resolved measurements of blood flow velocity fields. Several PC-MRI based methods for the estimation of WSS have been proposed (7-11). In principle, the WSS is estimated by using the velocity estimates in two or more adjacent voxels, sometimes combined with an estimation of the position of the wall. These methods are relatively easy to use and widely applied (9-10,12-13).

While PC-MRI velocity mapping measures an average of the velocities within each voxel, Fourier velocity encoding (FVE) MRI permits an estimation of the intravoxel velocity distribution by encoding a velocity k-space (k_v-space) in a manner similar to how spatial encoding is achieved. From this distribution, a subvoxel estimate of the position of the wall and the

velocity profile can be obtained, which can be used to estimate the WSS (14). Unfortunately, FVE acquisition times are long as one measurement is needed for every velocity encoding value, which also results in low temporal and spatial resolution. Recently, Carvalho et al (15) used spiral trajectories to speed up the acquisition of FVE data used for WSS estimation.

Another way of estimating the velocity gradient at a subvoxel level is by using intravoxel velocity standard deviation (IVSD) mapping, where the IVSD is estimated from the magnitude data of a PC-MRI measurement (16-19). This distribution can be used to estimate the spatial gradient in a voxel (17,19). The acquisition time of this technique is similar to conventional PC-MRI acquisitions.

The increasing number of studies that apply MRI based WSS estimation in-vivo (11-13,20-22) prompts the need for detailed investigations of the accuracy of the different techniques available. However, this is a challenging task considering that the true flow in a PC-MRI experiment is unknown and no gold standard for in-vivo flow measurements exists. Masaryk et al (23) investigated the accuracy of PC-MRI velocity-based techniques for WSS estimation in a straight tube and in-vivo in the internal carotid artery by comparison with a theoretically derived WSS estimate using Womersley's solution to the Navier-Stokes equation, and reported errors of up to 36%. Boussel et al (21) compared the results of PC-MRI velocity-based WSS estimation using an estimate of the vessel wall position with predictions from computational fluid dynamics and concluded that the approach used was insufficient for accurate WSS estimation. Stalder et al (11) introduced a velocity-based method comprising b-spline interpolation of velocities and segmentation of the vessel lumen and reported that MRI with a voxel length of 1 mm underestimates WSS by about 40% in a noise-free numerical simulation of parabolic flow with a

true WSS of 0.6 N/m^2 . They also demonstrated that MRI WSS estimates depend on the spatial resolution. Bieging et al (20) used 3D radially undersampled PC-MRI for WSS estimation, obtaining an increased spatial resolution (1 mm^3 isotropic voxels) which may result in an improved accuracy.

In addition to the spatial resolution, it is likely that also the voxel position relative to the wall (partial volume artifacts) and velocity encoding range (VENC) will affect MRI WSS estimates. To our knowledge, the impact of these parameters has not been systematically studied and, while several studies have demonstrated that MRI underestimates WSS, it is not known if the WSS estimates are monotonically related to the actual WSS, thus allowing relative WSS analysis. It was therefore the aim of this work to systematically study the accuracy of MRI WSS estimation. Specifically, we wanted to 1) compare the accuracy of different approaches available 2) investigate the impact of spatial resolution, voxel position, wall segmentation and VENC, and 3) investigate if MRI WSS estimates are monotonically related to the true WSS. Five conceptually different methods for WSS estimation, based on PC-MRI velocity mapping, FVE and IVSD mapping, were represented in the study.

METHODS

Simulations of MRI measurements based on numerical flow data allow for virtual measurements in a known flow field with known WSS values. To assess the sensitivity of MRI WSS estimation to different parameter settings, MRI measurements were simulated for a range of velocity profiles with different WSS values and the MRI WSS estimates obtained were compared to analytically derived WSS values. Five different methods were implemented: three based on PC-MRI velocity

mapping, the first using linear extrapolation (LE) (Vel-LE method), the second utilizing linear interpolation in combination with the position of the wall (Vel-Wall method), and the third utilizing parabolic fitting in combination with the position of the wall (Vel-Parabolic); one based on FVE (FVE method); and one based on IVSD mapping (IVSD method). The simulations were repeated for different settings of spatial resolution, voxel position, and VENC. Simple linear regression was used to investigate if there was a linear relationship between estimated and true WSS.

Flow Profiles

Twenty different two-dimensional velocity fields in a circular vessel with a diameter of 18 mm were considered. CFD studies of subject-specific geometries indicate that the magnitude of WSS in the normal human aorta and carotid artery ranges from 0-30 N/m^2 (24-25) and 0-5 N/m^2 (26), respectively. In the present study, WSS of 1 to 20 N/m^2 were considered. This was achieved by velocity profiles that were parabolic at the wall and flat in the center of the vessel (Figure 1). In this way, two-dimensional flow fields with analytically known WSS values (parabolic profile) and realistic peak velocities were obtained.

MRI Simulations

Velocity MRI measurements can be simulated in an accurate and straightforward manner by using an Eulerian-Lagrangian approach (27-29), but this is computationally expensive and would, even on a powerful workstation, require several days of computation time per simulation. To enable the investigation of a large number of parameter settings and flow conditions, simulations

were tailored to permit reasonable computation times (around 2 h for all combinations of voxel position, velocity profile and VENC for one voxel size and one method).
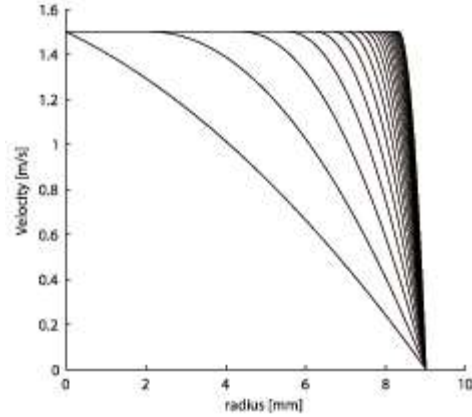
Figure 1 Plots of the 20 different velocity profiles considered in this study, with WSS values ranging from 1 to 20 N/m^2.

The MRI signal, $S(k_v)$, was simulated for a row of voxels along the radius of the vessel. Each voxel's point spread function (PSF) was computed and used to obtain the intravoxel velocity distribution, $s(v)$, from the 2D velocity field. The Fourier transform of $s(v)$ was computed to obtain the MRI signal, $S(k_v)$, where k_v is describes the first order motion sensitivity ($k_v = \gamma*M_1$, where M_1 is the first gradient moment). Noise and saturation effects were not simulated. In simulating the PC-MRI data needed for the IVSD method, a non-symmetric flow encoding scheme was used to obtain a motion sensitized flow encoding segment, $S(k_v)$ and a reference segment, $S(0)$. A symmetric encoding scheme was used to obtain the PC-MRI velocity data used in the Vel-LE method and the Vel-Wall method. The velocity and the IVSD were obtained from the phase and magnitude, respectively, of the complex-valued MRI signals. FVE measurements

were simulated by sampling the velocity distribution with different sampling intervals, Δv, over a velocity field of view of $\pm$ 1.5 m/s.

For the PC-MRI velocity based and FVE-based methods, a 2D PSF was defined as $jinc(sqrt(x^2+y^2)/\Delta r)$, corresponding to a radial or spiral acquisition, where Δr is the spatial resolution and x, y are the spatial coordinates. For the IVSD method, a Gaussian 2D PSF was created by taking the inverse Fourier transform of a Gaussian k-space filter. The voxels were placed along one of the coordinate axes and the normal of the wall, which is the ideal case for the Vel-LE method. In an in-vivo MRI measurement, the voxel position relative to the vessel wall and the amount of partial volume cannot be controlled and can thus be considered unknown, even if it can be estimated by segmentation of the vessel. Therefore, all simulations were carried out for ten different voxel positions uniformly distributed over one voxel length, thus covering the complete range of voxel positions in the direction of the wall's normal. The interval used for each method was chosen to include voxels positions that each method can handle, for example, for the FVE method only voxels containing both lumen and wall were considered.

For all methods except the FVE-based one, voxel sizes of 0.5, 1.0, and 1.5 mm were considered. This corresponds to 36, 18, and 12 voxels, respectively, across the diameter of an 18 mm diameter vessel. For the FVE-based method, voxel sizes of 3, 4 and 5 mm were used, corresponding to 6, 4.5 and 3.6 voxels across the diameter. The use of larger voxels for the FVE method is motivated by the time-consuming nature of this method. Smaller voxels require increased velocity resolution, which increases scan time (and computational time).

WSS Estimation

PC-MRI Velocity Mapping Linear Extrapolation Method

The estimates of the PC-MRI velocity based LE method (Vel-LE method), $WSS_{\text{Vel-LE}}$, were computed by using the velocity estimates from a voxel at the wall and the adjacent voxel in the direction towards the center of the vessel (9). The velocity estimates were unwrapped when needed. The LE method is based on the assumption of a linear velocity profile close to the wall and thus the spatial velocity derivative was estimated as the velocity difference between the two adjacent voxels divided by the distance between them, i.e. the voxel length (Figure 2 a). The distance between the wall and the center of the voxel located at the wall was varied stepwise from 0 to 1 voxel lengths, thus the voxel comprised up to 50% wall. $WSS_{\text{Vel-LE}}$ was obtained by multiplying the spatial velocity derivative with the dynamic viscosity of blood, which in this work was set to $4.6 \cdot 10^{-3}$ N·s/m^2.

PC-MRI Velocity Mapping with Wall Position Estimation

In an in-vivo measurement the wall position can be estimated by segmentation, and the estimated wall position in combination with PC-MRI velocity data can be used to estimate WSS (Vel-Wall method). This is the most commonly used approach today (11,20-22). We modeled this method by assuming the position of the wall to be known with a certain accuracy. The error of the wall position was assumed to be normally distributed with a standard deviation of 1/4 voxel size. Linear interpolation was used to obtain a velocity value, v_{interp}, at a specific distance, Δx, along the wall's inward normal. This distance was chosen to be one voxel length. The interpolated

velocity value was then divided by the distance from the wall to obtain the spatial velocity derivate and the WSS estimate, $WSS_{\text{Vel-Wall}}$ (Figure 2 b).

$$WSS_{Vel-Wall} = \mu \frac{v_{\text{int}erp}}{\Delta x}$$

The voxel position was varied in the same way as for the Vel-LE method.
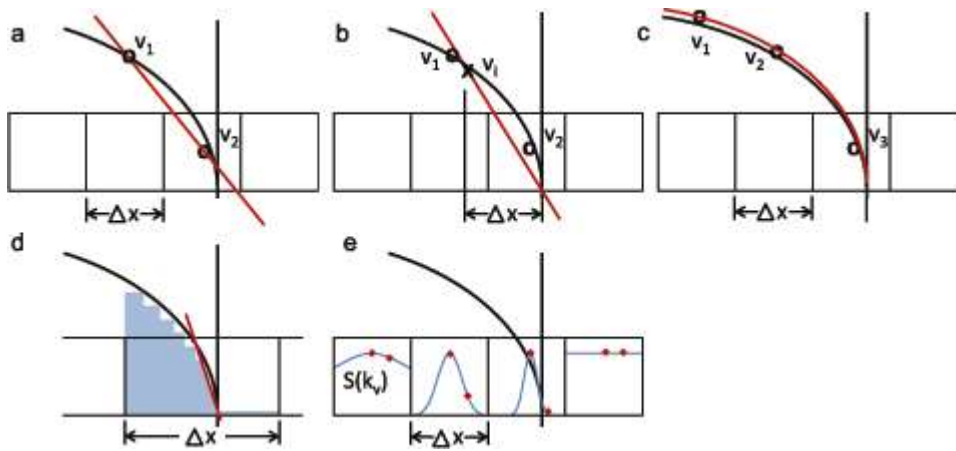
Figure 2 A schematic overview of the MRI-based WSS estimation methods included in this study. In all subpanels, a row of voxels of size Δx is illustrated. The vertical line represents the position of the wall and the curved black line represents the velocity profile. (a): Linear extrapolation method (Vel-LE method), where v_1 and v_2 are the measured mean velocities for the two voxels. The slope of the straight red line is used to obtain $WSS_{\text{Vel-LE}}$. (b): Velocity-based method utilizing the wall position (Vel-Wall), where v_i is the interpolated velocity at a distance Δx from the wall. The slope of the straight red line is used to obtain $WSS_{\text{Vel-Wall}}$. (c:) Velocity-based method utilizing parabolic fitting and the wall position (Vel-Parabolic), where a parabolic function is fitted to the velocity values of two voxels and the position of the wall. The spatial velocity derivative and $WSS_{\text{Vel-Parabolic}}$ is then analytically derived from the parabolic function. (d): The FVE method where the intravoxel velocity profile (seen in blue) is computed from the measured intravoxel velocity distribution and used to obtain WSS_{FVE}. (e): The IVSD method where $S(k_v)$ is sampled for two points, $k_v = 0$ and π/VENC. The relative signal loss between the two samples is then used to compute the IVSD and WSS_{IVSD}. The steeper velocity gradient, the more signal loss.

PC-MRI Velocity Mapping with Parabolic Fitting and Wall Position Estimation

To obtain a method that represents more advanced estimation (more degrees of freedom), a parabolic function was fitted to the position of the wall and the velocity values of two voxels close to the wall (Figure 2 c). This is similar to the method described by Oshinski et al (9). The wall position was estimated as in the Vel-Wall method described above. In order to make the estimates less sensitive to errors in segmentation, voxels with their center closer than a half voxel length from the wall were excluded from the parabolic fitting. The spatial velocity derivate at the wall was analytically derived from the fitted parabolic profile and used to obtain the WSS estimate, $WSS_{\text{Vel-Parabolic}}$. The voxel position was varied in the same way as for the Vel-LE and Vel-Wall methods.

Fourier Velocity Encoding Method

WSS estimation from the FVE simulations was performed following the approach proposed by Frayne et al (14) and Carvalho et al (15) (FVE method). The velocity distribution, $s(v)$, was sampled with the velocity sampling function defined as $sinc(v/\Delta v)$. The intravoxel velocity profile, $r(v)$ was computed as

$$r(v_i) = r(v_{i-1}) + \Delta r \cdot h(v_i) \text{, where, } h(v_i) = \frac{|s(v_i)|}{\sum |s(v)|}, \qquad \text{[Eq. 2]}$$

where Δr is the spatial resolution, and r is the intravoxel spatial position. From this intravoxel velocity profile, the spatial velocity derivative was estimated by fitting a straight line from the velocity values in a certain interval, $[v_0, v_1]$ (Figure 2 d). The interval was computed as $v_0 = \Delta v$ m/s and $v_1 = 4\Delta v$ m/s. WSS_{FVE} was only computed for voxels containing both wall and lumen,

thus the position of the voxel center was varied between ½ voxel length into the wall to ½ voxel length into the lumen.

PC-MRI Intravoxel Velocity Standard Deviation Mapping Method

IVSD-based WSS estimation (IVSD method) was performed based on the approach proposed by Pipe et al (19) and Dyverfeldt et al (16). This approach was extended by dividing the IVSD by a variable describing the spatial extent of the PSF. In this way, an estimate of the spatial velocity derivative in the voxel was obtained.

The IVSD, σ, which has been suggested to be monotonically related to WSS (19), is defined as the square root of the second central moment of the intravoxel velocity distribution.

$$\sigma = \sqrt{\left(\int_{-\infty}^{\infty} (v - \bar{v})^2 s(v) dv\right)} \ [\text{ms}^{-1}] \qquad \text{[Eq. 3]}$$

PC-MRI IVSD mapping is based on the assumption of a specific intravoxel velocity distribution, $s(v)$. For the estimation of WSS, we approximate the velocity profile as linear and one-directional in the region of interest close to the wall, resulting in a uniform velocity distribution in this region. A Gaussian k-space filter was used to obtain a Gaussian PSF. If the velocity distribution is constant over the extent of the voxel, the measured intravoxel velocity distribution will have the shape of a one-dimensional projection of the PSF, which in this case is a Gaussian function. In this way, the standard deviation of this Gaussian intravoxel velocity distribution can be obtained from the previously derived relationship (17-19)

$$\sigma = \sqrt{\frac{2\ln\left(|S(0)|/|S(k_v)|\right)}{k_v^2}} \ [\text{ms}^{-1}] \qquad \text{[Eq. 4]}$$

With the assumption of linear and one-directional velocity profiles, the velocity v can be expressed as

$$v = v' \cdot x + \bar{v} \quad (Eq.5)$$

where v' is the spatial velocity derivative, $\bar{v}$ is the mean velocity and x is the spatial coordinate in the direction of the gradient, $x = 0$ at the center of the voxel. By projecting the PSF to a one dimensional PSF, psf(x), and performing the variable substitution $x = (v - \bar{v})/v'$ the function $psf((v-\bar{v})/v')$ is obtained. This function describes the PSF-weighted velocity distribution of the voxel, i.e. $s(v) = psf((v-\bar{v})/v')$.

An estimate of the spatial velocity derivative, v', can be obtained by dividing the second central moment of $s(v)$ with the second moment of the $psf(x)$. The resulting quotient can be written as

$$\frac{\sigma^2}{\int_{-\infty}^{\infty} x^2 psf(x)dx} = \frac{\int_{-\infty}^{\infty} (v-\bar{v})^2 s(v)dv}{\int_{-\infty}^{\infty} x^2 psf(x)dx} = \frac{\int_{-\infty}^{\infty} (v-\bar{v})^2 s(v)dv}{\int_{-\infty}^{\infty} \frac{(v-\bar{v})^2}{v'^2} psf(\frac{(v-\bar{v})}{v'})dv} = v'^2 \quad \text{[Eq. 6]}$$

and thus

$$|v'| = \sqrt{\frac{\sigma^2}{\int_{-\infty}^{\infty} x^2 psf(x)dx}} \quad \text{[Eq. 7]}$$

The second moment of $psf(x)$ was computed by numerically integrating a high resolution representation of $psf(x)$. An estimate of the WSS was obtained by multiplying $|v'|$ with the dynamic viscosity according to equation 1.

WSS was computed for two adjacent voxels and the largest estimate was chosen as WSS_{IVSD}. As for the FVE method, the position of the outermost voxel center was varied from ½ voxel length inside the wall to ½ voxel length inside the lumen, thus excluding voxels with only wall. In Figure 2 e the influence of WSS on the MRI signal, $S(k_v)$, is illustrated.

WSS Analysis

Simple linear regression was used to test for a linear relationship and correlation between the estimated WSS and the true WSS. A least-squares estimation was used to compute the linear regression model, $WSS_{estimate} = \beta \cdot WSS$. The estimate for a WSS of 0 was assumed to be 0 and thus no intercept was used. Consequently, the coefficient of determination, R^2, may also be negative when the fit is very poor. As higher WSS values are more difficult to resolve due to limited spatial resolution, regression analysis was done for two WSS intervals 1-5 and 1-20 N/m^2, representing the expected WSS range in a healthy carotid bifurcation and a healthy aorta, respectively. A t-test was used to test the null hypothesis that the slope, β, is equal to zero.

RESULTS

The estimated WSS using all five approaches for typical acquisition parameters is shown in Figure 3. The linear regression analysis for the whole interval 0-20 N/m^2 (Table 1) generally showed a very weak linear relationship for all methods (for VENC = 2 m/s and Δv = 0.15 m/s). However, the Vel-Parabolic method with a spatial resolution of 0.5 mm showed a moderate linear relationship (β=0.95, R^2=0.53). For the FVE method the slope of the regression line was close to 1, but the linear relationship was poor (β=1.00, R^2=0.20 for 3 mm voxels).
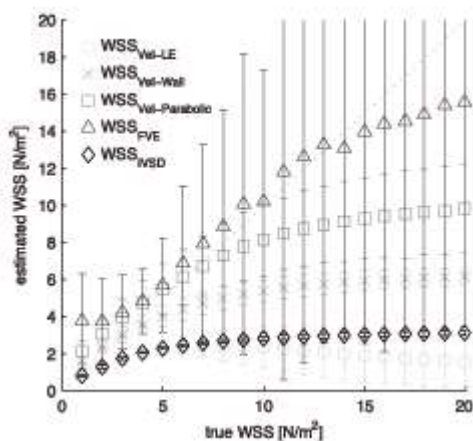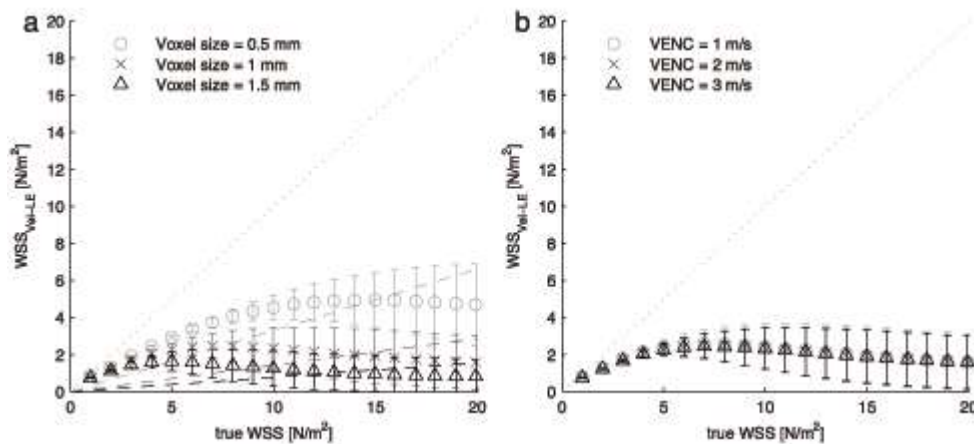
Figure 3 Plots of the WSS estimates obtained using all five methods. For the PC-MRI velocity (WSS_{Vel-LE}, $WSS_{Vel-Wall}$, $WSS_{Vel-Parabolic}$) and IVSD (WSS_{IVSD}) based methods the voxel size was 1 mm and the VENC 2 m/s. For the FVE based method (WSS_{FVE}) the voxel size is 4 mm and Δv 0.15 m/s. The vertical axis shows the estimated WSS and the horizontal axis shows the analytically derived WSS values. The error bars show the standard deviation due to voxel position relative the wall and wall position estimate inaccuracy; 10 different voxel positions were simulated.

The Vel-LE, Vel-Wall, Vel-Parabolic and IVSD methods generally performed better in the linear regression analysis of the lower interval, 1-5 N/m^2 (Table 1). However, the FVE method and the Vel-Parabolic method for a voxel size of 0.5 mm performed less good in this interval as WSS was overestimated. For the Vel-LE method a strong linear relationship between WSS_{Vel-LE} and actual WSS was obtained for a spatial resolution of 0.5 mm for actual WSS = 0-5 N/m^2, (β=0.62, R^2=0.96). Regression lines for the entire interval are shown in Figure 4. The estimates from the velocity-based method utilizing the wall positon, $WSS_{Vel-Wall}$, and the corresponding regression lines are shown in Figure 5. In an interval of 0-5 N/m^2 there was a moderate linear relationship between $WSS_{Vel-Wall}$ and the true WSS (β=0.90, R^2=0.56 for 1 mm voxels). The estimates from

the method based on parabolic fitting, $WSS_{Vel-Parabolic}$, are shown in Figure 6, and are higher than $WSS_{Vel-Wall}$. The Vel-Parabolic method overestimated WSS for low WSS (0-5 N/m^2). The estimates from the FVE method, WSS_{FVE}, (Figure 7) appear to be non-linearly related to the actual WSS ($R^2 < 0.21$ for all intervals) and even negative R^2 values were present. The IVSD method performed similarly as the velocity-based method (Figure 8). The p-value from the t-test was less than 0.05 for all tested intervals, thus rejecting the null hypothesis that β is zero.

Figure 4 Plots of the WSS estimates obtained using the Vel-LE method. (a): WSS_{Vel-LE} for three different voxel sizes, 0.5, 1.5, 2.0 mm, for a VENC of 2 m/s. (b): WSS_{Vel-LE} for three different VENC, 1 m/s, 2 m/s, 3 m/s, for a voxel size of 1 mm. The vertical axis shows the estimated WSS and the horizontal axis shows the analytically derived WSS values. The error bars show the standard deviation due to voxel position relative the wall; 10 different voxel positions were simulated and the distance from the wall to the voxel center was varied from 0 to 1 of the voxel length into the lumen. In (a), the identity line (dotted) and the linear regression line for each voxel size (dashed) are included.

For all velocity profiles and parameter settings studied, the Vel-LE method and IVSD method underestimated the WSS (Figures 4 and 8). The Vel-Wall and the Vel-Parabolic methods slightly overestimated WSS for low WSS (Figure 5, Figure 6) and underestimated high WSS values. For all five methods, the estimated WSS as a function of voxel position relative the wall is shown in

Figure 9; the actual WSS is 4 and 8 N/m^2. Voxel position only had minor influence on the velocity and IVSD based methods, but influenced WSS_{FVE} considerably.
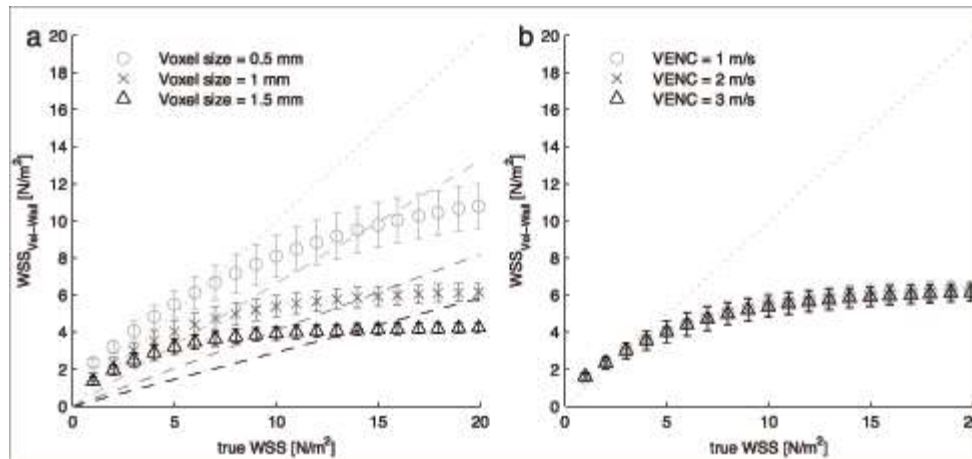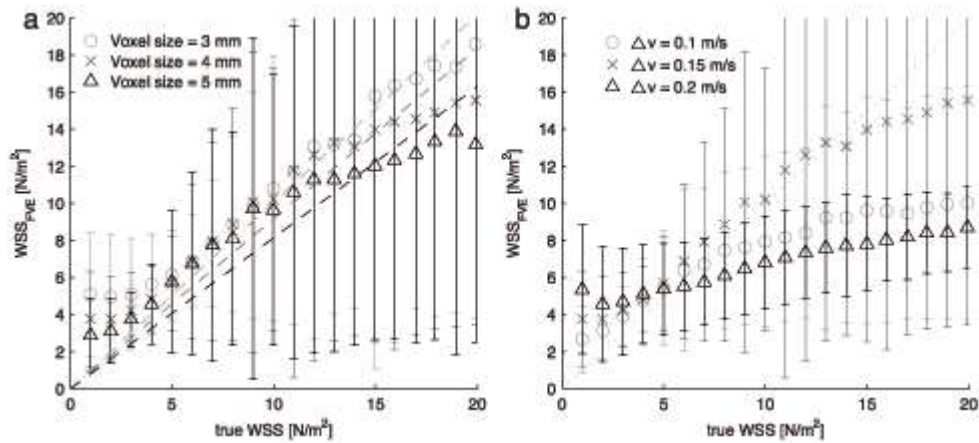

Figure 5 Plots of the WSS estimates obtained using the Vel-Wall method. (a): $WSS_{\text{Vel-Wall}}$ estimates for three different voxel sizes, 0.5, 1.5, 2.0 mm, for a VENC of 2 m/s. (b): $WSS_{\text{Vel-Wall}}$ estimates for three different VENC, 1 m/s, 2 m/s, 3 m/s, for a voxel size of 1 mm. The vertical axis shows the estimated WSS and the horizontal axis shows the analytically derived WSS values. The error bars show the standard deviation due to voxel position relative the wall and wall position estimate inaccuracy; 10 different voxel positions were simulated and the distance from the wall to the voxel center was varied from 0 to 1 of the voxel length into the lumen. The position of the wall was assumed to be known with certain accuracy (standard deviation 1/4 voxel size). In (a), the identity line (dotted) and the linear regression line for each voxel size (dashed) are included.

For all methods except the FVE method, high WSS values were poorly resolved. For example, when using voxel lengths of 0.5 and 1 mm, WSS values over 10 and 3 N/m^2, respectively, could not be resolved with the Vel-LE method. The underestimation depended mainly on voxel size, as seen from Figure 4-6a and 8a. The VENC setting generally had a minor impact on the estimates,

although WSS_{IVSD} obtained with a VENC of 1 m/s were less accurate for WSS values over 5 N/m^2 than estimates obtained with a higher VENC. WSS_{IVSD} using a VENC of 1 m/s even had a negative slope for large WSS (Figure 8). The voxel position had minor effects on $WSS_{Vel-Wall}$ and $WSS_{Vel-Parabolic}$ (Figure 9), but uncertainty in the estimation of the wall position (segmentation) introduced non-negligable errors (Figures 5-6a).
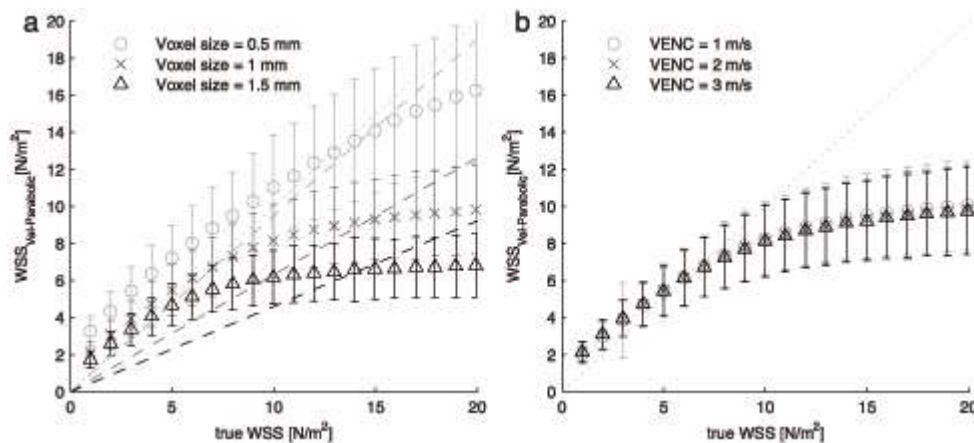

Figure 6 Plots of the WSS estimates obtained using the Vel-Parabolic method. (a): $WSS_{Vel-Parabolic}$ estimates for three different voxel sizes, 0.5, 1.5, 2.0 mm, for a VENC of 2 m/s. (b): $WSS_{Vel-Parabolic}$ estimates for three different VENC, 1 m/s, 2 m/s, 3 m/s, for a voxel size of 1 mm. The vertical axis shows the estimated WSS and the horizontal axis shows the analytically derived WSS values. The error bars show the standard deviation due to voxel position relative the wall and wall position estimate inaccuracy; 10 different voxel positions were simulated and the distance from the wall to the voxel center was varied from 0 to 1 of the voxel length into the lumen. The position of the wall was assumed to be known with certain accuracy (standard deviation 1/4 voxel size). In (a), the identity line (dotted) and the linear regression line for each voxel size (dashed) are included.

Figure 7 Plots of the WSS estimates obtained using the FVE method. (a): WSS_{FVE} for three different voxel sizes, 3, 4, 5 mm, for a Δv of 0.15 m/s. (b): WSS_{FVE} for three different Δv, 0.1 m/s, 0.15 m/s, 0.2 m/s, for a voxel size of 4 mm. The vertical axis shows the estimated WSS and the horizontal axis shows the analytically derived WSS values. The error bars show the standard deviation due to voxel position relative the wall; 10 different voxel positions were simulated and the distance from the wall to the voxel center was varied from -½ to ½ of the voxel length into the lumen. In (a), the identity line (dotted) and the linear regression line for each voxel size (dashed) are included.
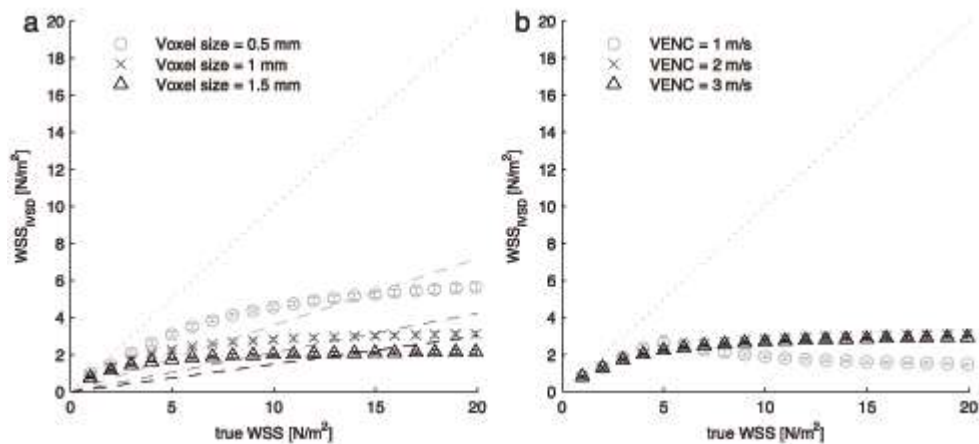
Figure 8 Plots of the WSS estimates obtained using the IVSD method. (a): WSS_{IVSD} for three different voxel sizes, 0.5, 1.5, 2.0 mm, for a VENC of 2 m/s. (b): WSS_{IVSD} for three different VENC, 1 m/s, 2 m/s, 3 m/s, for a voxel size of 1 mm. The vertical axis shows the estimated WSS and the horizontal axis shows the analytically derived WSS values. The error bars show the standard deviation due to voxel position relative the wall; 10 different voxel positions were simulated and the distance from the wall to the voxel center was varied from -½ to ½ of the voxel length into the lumen. In (a), the identity line (dotted) and the linear regression line for each voxel size (dashed) are included
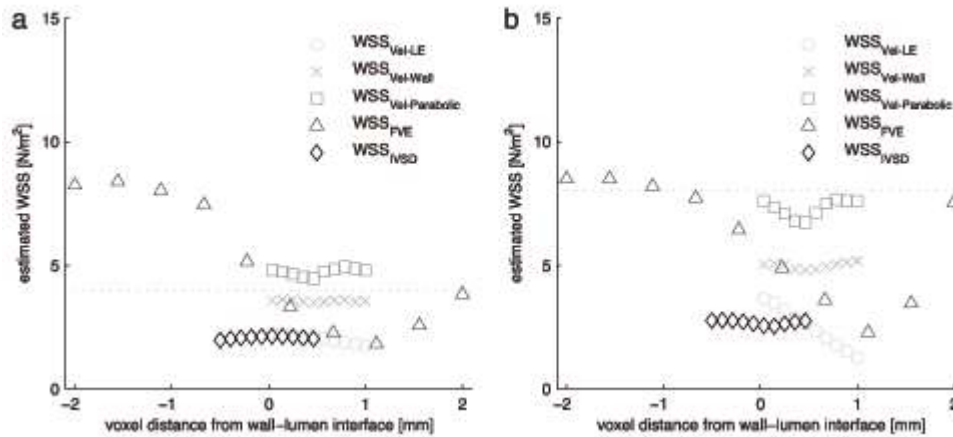
Figure 9 Plots of the estimated WSS as a function of voxel position for all four methods for a single velocity profile with a WSS of a) 4 N/m^2 and b) 8 N/m^2. For the PC-MRI velocity (WSS_{Vel-LE}, $WSS_{Vel-Wall}$, $WSS_{Vel-Parabolic}$) and IVSD (WSS_{IVSD}) based methods the voxel size was 1 mm and the VENC 2 m/s. For the FVE based method (WSS_{FVE}) the voxel size is 4 mm and Δv 0.15 m/s. The vertical axis shows the estimated WSS and the horizontal axis shows the distance between the voxel center and the wall-lumen interface; positive values are in the lumen and negative values are in the wall.

Although the mean values of WSS_{FVE} are accurate, large errors (percentage errors above 300%) were seen for suboptimal parameter settings (Figure 7). Errors in the FVE method appear less predictable than for the other methods studied. Especially when the voxel edge was placed at the lumen-wall interface, large errors were seen (Figure 9).

DISCUSSION

This study investigated the accuracy of MRI-based WSS estimation by using numerical MRI simulations. Methods based on PC-MRI velocity mapping (one using linear extrapolation, one

also utilizing the wall position and one utilizing fitting of a parabolic function), FVE, and IVSD data were included and the influence of spatial resolution, velocity encoding settings, segmentation errors and voxel location relative to the wall were investigated for different flow profiles.

In general, the methods based on PC-MRI velocity mapping (Vel-LE method, Vel-Wall method and Vel-Parabolic) underestimated WSS (although Vel-Parabolic overestimated low WSS). Spatial resolution considerably influenced all methods. The estimated wall position (segmentation) severely influenced $WSS_{\text{Vel-Parabolic}}$ (Figure 6), but the Vel-Parabolic method was the most accurate over the entire interval (WSS = 1-20 N/m^2). The FVE method was very sensitive to parameter settings and the voxel position had a large influence on the errors (Figure 7, Figure 9). Thus, varying voxel position relative the wall, e.g. motion of the vessel wall or positioning of the field of view will cause the WSS estimates to vary even if there is no actual change in flow. The linear relationship between WSS_{FVE} and actual WSS was weak (Table 1). The accuracy of the IVSD method is comparable to the Vel-LE method (Figure 4, 8, Table 1).

Our results regarding the Vel-LE, Vel-Wall, and Vel-Parabolic methods are in line with those obtained in previous studies of the accuracy of velocity-based WSS estimation, where MRI has been reported to underestimate the true WSS (11,23). In addition, we found that the degree of underestimation depended on the actual WSS. Spatial resolution had the most significant impact on the accuracy of the estimates. Obviously, this will severely hamper the comparison of WSS estimates obtained from datasets with different resolution. Also, these findings indicate that comparisons of WSS estimates in different directions in an anisotropic velocity data set should be handled with great care. For example, if using an anisotropic voxel size of 1 mm x 1.5 mm, the

mean of $WSS_{\text{Vel-Wall}}$ for a true WSS of 10 N/m^2 can vary between 5.39 N/m^2 and 3.94 N/m^2 due to the direction of the velocity gradient (Figure 5 a).

In this work, the voxels were positioned along the wall's normal direction. If the voxels are not oriented in this way, the Vel-LE method may produce even less accurate results. This is accounted for in more advanced PC-MRI velocity-based methods, for example, by using sectored 3D parabolic fitting (30) or B-spline interpolation (11). As these methods utilize the large parts of the flow field, rather than a few adjacent voxels, they are presumably less sensitive to noise. However, they can be expected to suffer from the same principal problems as those seen here for the Vel-Parabolic method. Furthermore, imposing more assumptions on the velocity profile may decrease the accuracy for realistic (more complex) flow profiles.

In our study, the FVE method was capable of providing accurate results for some parameter settings and voxel positions, but as seen in Figures 3,7 and 9, errors were more severe when voxel size and Δv settings were suboptimal. In our experience, no single FVE settings would have resulted in accurate WSS estimates for all flow profiles evaluated. Choosing voxel size for the FVE method is non-trivial. While large voxels imply spatial averaging, the use of smaller voxels necessitates higher velocity resolution. When the voxels are small and the velocity resolution is insufficient, too few velocity samples containing signal may be acquired. Furthermore, if the voxel is placed further away from the lumen-wall interface, such as at edge of this interface, the signal from the lower velocities close to the wall will be lower than expected due to the shape of the PSF, resulting in a poorly estimated velocity profile close to the wall and, as a result, inaccurate WSS estimates. However, if a lower velocity resolution is used, these low velocities will not be as important as the WSS is estimated further away from the wall; this is

exemplified by the use of $v_0 = \Delta v$ m/s and $v_1 = 4\Delta v$ m/s in this study. The FVE method may be improved by compensating for the shape of the PSF (15), which remains a challenge. However, it would still be very difficult to obtain accurate WSS values when the magnitude of the PSF is low at the lumen-wall interface, as noise may be amplified by the compensation. A multigrid approach could potentially increase the accuracy of the FVE method. For example, in the worst case scenario where the wall-lumen interface is right between two voxels, FVE data may also be reconstructed at half the spatial resolution to obtain a (large) voxel with its center at the wall-lumen interface. For a WSS of 5 N/m^2, $\Delta v = 0.15$ m/s and voxel size 3 mm, WSS_{FVE} for two adjacent voxels placed on each side of the lumen-wall interface would be 6.73 and 8.82 N/m^2, respectively, and for a 6 mm voxel centered at the interface WSS_{FVE} would be 3.91 N/m^2. Previous studies using simulations of FVE measurements of the flow in the carotid artery have shown promising results for the FVE-based method (15). Conceptually, the FVE method has the potential to produce the most accurate estimates, but it is hampered by long acquisition times as well as sensitivity to voxel size, velocity resolution and voxel position. Possibly, a compromise between the IVSD method and the FVE method could address these drawbacks.

The IVSD method appears to be slightly more sensitive to VENC than the PC-MRI velocity based methods (Figure 8 b). However, when compared to the PC-MRI velocity-based estimation of WSS, the IVSD method does have some appealing features: it will handle any geometry of the vessel, estimates do not depend on segmentation, it may be less sensitive to assumptions about the velocity profile, and voxel-by-voxel WSS estimates are obtained. Note that Vel-LE and IVSD WSS estimates can be obtained from the same PC-MRI acquisition (17), which allows also for a combination of these approaches. However, the IVSD WSS method is not recommended for

disturbed flows as phase-dispersion caused by fluctuating velocities would violate the underlying assumptions.

The present study did not investigate the effects of noise and only relatively simple velocity profiles were considered. This implies that the WSS estimates presented here represent a best case scenario. PC-MRI velocity based WSS estimation based on B-spline interpolation has been shown to be relatively insensitive to noise, with errors due to noise being about two orders of magnitude smaller than the WSS estimates (11). The IVSD method will be sensitive to noise when the WSS induced signal loss is either very low or very high. Another limitation of the simulations performed in this study was that saturation effects were not taken into account, although this effect should be minor for 3D acquisitions. It should also be noted that only simple geometries were considered. The geometries and the velocity profiles will be far more complex in-vivo, the wall will move, and the flow will be pulsatile. Retrograde flow and skewed velocity profiles can be present, especially under abnormal flow conditions. It is likely that this will further decrease the accuracy of the WSS estimates. Consequently, it is very difficult to measure WSS using a method limited by the spatiotemporal resolution of MRI. WSS is commonly computed from aortic 4D PC-MRI, and voxels are seldom smaller than 2 x 2 x 2 mm^3. Large voxels will result in less accurate results and high WSS values will then be even more difficult to differentiate. Further investigations on acquisition and post-processing strategies are therefore necessary before these techniques can be applied to accurately measure WSS in patient studies. We speculate that a combination of velocity, FVE and IVSD based WSS estimation, may be helpful in advancing MRI WSS estimation. By using both the magnitude and phase of the PC-MRI signal a less noise sensitive method may be developed. The challenges associated with

imaging-based WSS estimation has led to the popularity of subject-specific image-based CFD modeling for WSS computation (6,21,25,31), which offers a very high spatial resolution close to the wall but is often limited by assumptions about rigid walls. An intriguing option for future research is to estimate WSS based on a hybrid CFD and 4D PC-MRI approach.

Notwithstanding the fact that the accuracy of MRI based WSS estimation is low, the technique may still be useful when used with care. In-vivo WSS estimates may be compared relative to each other. In this way, areas with low and high WSS may be differentiated (11,13,22). However, the results obtained in the present study highlight that anisotropic voxels, as well as differences in voxel location and flow profile may lead to large errors. Thus, it is recommended that only WSS estimates obtained from measurements with the same isotropic resolution are compared. A subject-specific CFD study of the flow in a healthy carotid bifurcation indicates that WSS values up to 5 N/m^2 may be present (26). In a severely stenotic carotid bifurcation, WSS values up to 70 N/m^2 have been reported (32). WSS in giant cerebral aneurysms may be up to 2-5 N/m^2 (33-34) and peak WSS in the normal human aorta is reportedly 30 N/m^2 (24-25). Thus, the methods used in this work will only be accurate for a limited number of clinical cases. For example, in the presence of stenotic jets or turbulent fluctuations near the wall, the accuracy of MRI WSS estimation can be expected to be low. However, as studies have indicated that low WSS is involved in both aneurysm growth (6) and the formation of atherosclerotic plaques (2), it may not always be necessary to accurately estimate high WSS. Noteworthy, the assessment of vectorial WSS may be compromised by the inability to resolve high WSS. For example, if using the Vel-LE method with a spatial resolution of 1 mm and the WSS vector is made up of two vector components, with WSS values of 3 and 10 N/m^2 respectively, both estimates will be around 3

N/m^2 and both the direction and the magnitude of the estimated WSS vector will be incorrect. If absolute WSS values are of interest, the FVE method may be considered, although due to its unstable performance in the present study, Vel-Wall or Vel-Parabolic method using a high spatial resolution (at least 0.5 mm) may be the best choice.

In conclusion, this study performed simulations to assess the accuracy of PC-MRI and FVE based approaches for WSS estimation. Even in the absence of noise and for relatively simple velocity profiles, all methods evaluated were found to be impacted by considerable errors depending on parameter settings such as VENC, velocity resolution, and especially spatial resolution. Furthermore, MRI WSS estimates cannot always be assumed to be linearly or even monotonically related to actual WSS. PC-MRI velocity based WSS estimation utilizing information about the position of the wall produced the most accurate estimates. However, high WSS values are not well resolved and the estimates depend on the position of voxels relative to the wall and errors in the estimation of the wall position. Nevertheless, velocity PC-MRI acquired with isotropic resolution may be useful in distinguishing areas of low and moderate WSS.

ACKNOWLEDGEMENT

References

1. Brooks AR, Lelkes PI, Rubanyi GM. Gene expression profiling of human aortic endothelial cells exposed to disturbed flow and steady laminar flow. Physiological genomics 2002;9(1):27.
2. Cheng C, Tempel D, van Haperen R, et al. Atherosclerotic lesion size and vulnerability are determined by patterns of fluid shear stress. Circulation 2006;113(23):2744.

3.   Malek A, Alper S, Izumo S. Hemodynamic shear stress and its role in atherosclerosis. Jama 1999;282(21):2035.

4.   Reneman RS, Arts T, Hoeks APG. Wall shear stress–an important determinant of endothelial cell function and structure–in the arterial system in vivo. Journal of vascular research 2006;43(3):251-269.

5.   Shaaban A, Duerinckx A. Wall Shear Stress and Early Atherosclerosis A Review. American Journal of Roentgenology. Volume 174: Am Roentgen Ray Soc; 2000. p 1657-1665.

6.   Boussel L, Rayz V, McCulloch C, et al. Aneurysm growth occurs at region of low wall shear stress. Stroke 2008;39(11):2997-3002.

7.   Cheng CP, Parker D, Taylor CA. Quantification of wall shear stress in large blood vessels using Lagrangian interpolation functions with cine phase-contrast magnetic resonance imaging. Annals of Biomedical Engineering 2002;30(8):1020-1032.

8.   Lou Z, Yang W, Stein P. Errors in the estimation of arterial wall shear rates that result from curve fitting of velocity profiles. Journal of biomechanics 1993;26(4-5):383-390.

9.   Oshinski J, Ku D, Mukundan Jr S, Loth F, Pettigrew R. Determination of wall shear stress in the aorta with the use of MR phase velocity mapping. Journal of Magnetic Resonance Imaging 1995;5(6):640-647.

10.   Oyre S, Pedersen E, Ringgaard S, Boesiger P, Paaske W. In vivo wall shear stress measured by magnetic resonance velocity mapping in the normal human abdominal aorta*. European Journal of Vascular and Endovascular Surgery 1997;13(3):263-271.

11.   Stalder A, Russe M, Frydrychowicz A, Bock J, Hennig J, Markl M. Quantitative 2D and 3D phase contrast MRI: optimized analysis of blood flow and vessel wall parameters. Magnetic Resonance in Medicine 2008;60(5):1218-1231.

12.   Barker A, Lanning C, Shandas R. Quantification of Hemodynamic Wall Shear Stress in Patients with Bicuspid Aortic Valve Using Phase-Contrast MRI. Annals of Biomedical Engineering 2010;38(3):788-800.

13.   Harloff A, Nußbaumer A, Bauer S, et al. In vivo assessment of wall shear stress in the atherosclerotic aorta using flow sensitive 4D MRI. Magnetic Resonance in Medicine 2010;63(6):1529-1536.

14.   Frayne R, Rutt B. Measurement of fluid-shear rate by Fourier-encoded velocity imaging. Magnetic Resonance in Medicine 1995;34(3):378-388.

15.   Carvalho J, Nielsen J, Nayak K. Feasibility of in vivo measurement of carotid wall shear rate using spiral fourier velocity encoded MRI. Magnetic Resonance in Medicine 2010;63(6):1537-1547.

16.   Dyverfeldt P, Sigfridsson A, Knutsson H, Ebbers T. A novel MRI framework for the quantification of any moment of arbitrary velocity distributions. Magnetic Resonance in Medicine 2011;65(3):725-731.

17.   Dyverfeldt P, Sigfridsson A, Kvitting J, Ebbers T. Quantification of intravoxel velocity standard deviation and turbulence intensity by generalizing phase-contrast MRI. Magnetic Resonance in Medicine 2006;56(4):850-858.

18.   Gao J, Gore J. Turbulent flow effects on NMR imaging: measurement of turbulent intensity. Medical Physics 1991;18:1045.

19.   Pipe J. A simple measure of flow disorder and wall shear stress in phase contrast MRI. Magnetic Resonance in Medicine 2003;49(3):543-550.

20. Bieging ET, Frydrychowicz A, Wentland A, et al. In vivo three dimensional MR wall shear stress estimation in ascending aortic dilatation. Journal of Magnetic Resonance Imaging 2011;33(3):589-597.

21. Boussel L, Rayz V, Martin A, et al. Phase contrast magnetic resonance imaging measurements in intracranial aneurysms in vivo of flow patterns, velocity fields, and wall shear stress: Comparison with computational fluid dynamics. Magnetic Resonance in Medicine 2009;61(2):409-417.

22. Markl M, Wallis W, Harloff A. Reproducibility of flow and wall shear stress analysis using flow-sensitive four-dimensional MRI. Journal of Magnetic Resonance Imaging 2011;33(4):988-994.

23. Masaryk A, Frayne R, Unal O, Krupinski E, Strother C. In vitro and in vivo comparison of three MR measurement methods for calculating vascular shear stress in the internal carotid artery. American Journal of Neuroradiology 1999;20(2):237.

24. Leuprecht A, Kozerke S, Boesiger P, Perktold K. Blood flow in the human ascending aorta: a combined MRI and CFD study. Journal of engineering mathematics 2003;47(3):387-404.

25. Renner J, Gårdhagen R, Ebbers T, Heiberg E, Länne T, Karlsson M. A method for subject specific estimation of aortic wall shear stress. WSEAS Transactions on Biology and Biomedicine 2009;6(3):49-57.

26. Steinman DA, Thomas JB, Ladak HM, Milner JS, Rutt BK, Spence JD. Reconstruction of carotid bifurcation hemodynamics and wall thickness using computational fluid dynamics and MRI. Magnetic Resonance in Medicine 2002;47(1):149-159.

27. Lee KL, Doorly DJ, Firmin DN. Numerical simulations of phase contrast velocity mapping of complex flows in an anatomically realistic bypass graft geometry. Medical Physics 2006;33(7):2621-2631.

28. Marshall I. Computational simulations and experimental studies of 3D phase contrast imaging of fluid flow in carotid bifurcation geometries. Journal of Magnetic Resonance Imaging 2010;31(4):928-934.

29. Petersson S, Dyverfeldt P, Gårdhagen R, Karlsson M, Ebbers T. Simulation of phase contrast MRI of turbulent flow. Magnetic Resonance in Medicine 2010;64(4):1039-1046.

30. Oyre S, Ringgaard S, Kozerke S, et al. Quantitation of circumferential subpixel vessel wall position and wall shear stress by multiple sectored three-dimensional paraboloid modeling of velocity encoded cine MR. Magnetic Resonance in Medicine 1998;40(5):645-655.

31. Steinman DA, Taylor CA. Flow imaging and computing: large artery hemodynamics. Annals of Biomedical Engineering 2005;33(12):1704-1709.

32. Stroud J, Berger S, Saloner D. Numerical analysis of flow through a severely stenotic carotid artery bifurcation. Journal of Biomechanical Engineering 2002;124:9.

33. Jou LD, Quick CM, Young WL, et al. Computational approach to quantifying hemodynamic forces in giant cerebral aneurysms. American Journal of Neuroradiology 2003;24(9):1804.

34. Steinman DA, Milner JS, Norley CJ, Lownie SP, Holdsworth DW. Image-based computational simulation of flow dynamics in a giant intracranial aneurysm. American Journal of Neuroradiology 2003;24(4):559.

Table 1. Linear regression results for two intervals 1-5 and 1-20 N/m^2 for all methods.

Method	Voxel Size [mm]	R^2 (1-5 N/m^2)	β (1-5 N/m^2)	R^2 (1-20 N/m^2)	β (1-20 N/m^2)
WSS$_{Vel-LE}$	0.5	0.96	0.62	0.15	0.33
WSS$_{Vel-LE}$	1	0.77	0.51	-0.70	0.14
WSS$_{Vel-LE}$	1.5	0.16	0.40	-0.73	0.08
WSS$_{Vel-Wall}$	0.5	0.51	1.23	0.31	0.64
WSS$_{Vel-Wall}$	1	0.56	0.90	-0.09	0.40
WSS$_{Vel-Wall}$	1.5	0.49	0.74	-0.73	0.29
WSS$_{Vel-Parabolic}$	0.5	0.26	1.63	0.53	0.95
WSS$_{Vel-Parabolic}$	1	0.44	1.21	0.24	0.63
WSS$_{Vel-Parabolic}$	1.5	0.47	1.03	-0.17	0.46
WSS$_{FVE}$	3	-0.44	1.52	0.20	1.00
WSS$_{FVE}$	4	-0.22	1.31	0.17	0.92
WSS$_{FVE}$	5	0.07	1.23	0.14	0.82
WSS$_{IVSD}$	0.5	0.92	0.66	0.51	0.36
WSS$_{IVSD}$	1	0.78	0.52	-0.72	0.21
WSS$_{IVSD}$	1.5	0.39	0.41	-2.39	0.15

R^2 is the coefficient of determination and β is the derivative of the regression model. The p-value from the t-test was below 0.05 in all cases. The VENC was 2 m/s and Δv was 0.15 m/s.